Proceedings of DETC'00
26th Biennial Mechanisms and Robotics Conference
September 10-13, 2000, Baltimore, Maryland, USA

DETC2000/MECH-6821

SIMULATING CERVICAL VERTEBRAE MOTION USING ELEMENTARY CONTACT PAIRS

Andrés Kecskeméthy*
Institut für Mechanik
und Getriebelehre
Technische Universität Graz
A-8010 Graz
Austria
Email: kecskemethy@mechanik.tu-graz.ac.at

Christian Lange, Gerald Grabner
Institut für Mechanik
und Getriebelehre
Technische Universität Graz
A-8010 Graz
Austria
Email: {lange|grabner}@mechanik.tu-graz.ac.at

ABSTRACT

Described in the paper is the mathematical modeling of a vertebrae pair using multibody methods and impact analysis techniques with elementary contact geometry for the facet joints. The results are compared with existing approaches and with experimental data, showing a good agreement with the latter and an efficiency boost compared to existing approaches by a factor of 350. The investigations are focused on the vertebrae pair C5–C6 but can be easily extended to other vertebrae.

Introduction

In the reduction of medical costs, the improvement of human disease therapies, the development of new techniques for injury prevention measures, and many other fields related to human life, biomechanics is playing an increasingly important role. Areas of actual research in this setting are, among others, the development and surgical placement of spinal prosthetic devices such as spine implants, effective spinal immobilizers and spine braces (DiAngelo et al. 1996), design of reliable anthropomorphic test devices (ATD) for physical crashworthiness simulations (Wismans et al. 1986), and the *in vivo* and *in vitro* estimation of biological spine parameters (Bilston and Thibault 1996, Margulies et al. 1992). In this setting, reconstruction of inter-vertebral motion, although basically understood, still poses many open problems. This is so because pairs of vertebrae undergo in general six-dimensional motion relative to one another, but display a high degree of coupling between gross translational and rotational degrees-of-freedom due to restraints imposed by ligaments and muscles and the compliant nature of the inter-vertebral discs (White and Panjabi 1990). These degrees of freedom are excited differently depending on loading conditions and biological parameters, making it difficult to establish relevant kinematic parameters on a case-by-case basis, as required, e.g., to identify spinal diseases or to mimic the effects of a surgical therapy for a concrete person. Hence, predictions often fail to match experimental measurements, as is the case in particular in vehicle crash situations (Geigl et al. 1995).

Existing approaches for computer modelling of inter-vertebral motion use either kinematic or full-scale finite element (FEM) models to reproduce vertebrae interaction. Kinematic methods regard mainly planar flexion and extension motion in the sagittal plane, employing the notion of instantaneous axes of rotation (IAR) to reproduce combined rotation and translation between pairs of vertebrae (White and Panjabi 1990). These axes act as virtual hinges connecting pairs of vertebrae, where the virtual pivot point is located somewhere between the centers of the two connected vertebrae and the center of the inter-vertebral disc (Jansen and DiAngelo 1997). They embody the well-known first-order approximation of planar motion in kinematics (Bothema and Roth 1990). The problem with this approach is that the location of the IAR varies with respect to flexural position as well as with respect to clinical and personal data (age, sex) of the tar-

* Address all correspondence to this author.

get person. Moreover, the IAR approach is not easily extendible to full-degree-of-freedom joints, such as occurs in a combined flexion-extension and lateral or axial rotation of the spine. On the other hand, FEM modelling allows one to take into consideration full effects of the mechanics of inter-vertebral motion, including contact mechanics, surface gliding, and deformation. For such models, a number of now industry-standard programs have been developed, such as MADYMO (Lupker et al. 1991), ATB (Obergefell et al. 1988), and LS-DYNA3D (Bedewi and Bedewi 1996). However, these models have the drawback that for actual computations, a great number of biological parameters are required that are difficult to impossible to obtain. Moreover, the computer models are computationally very slow, prohibiting their use for real-time simulations, as required for educational or optimization purposes. This also hampers their immediate use in medical applications, where fast, online rendering of motion properties is necessary to assess the effects of therapeutic measures.

This paper deals with the mechanical modelling of the motion only between one pair of vertebrae of the human cervical spine, namely C5–C6. However, the underlying theory is developed in such a general way that other vertebrae pairs can be rapidly modeled correspondingly, when needed.

Basic Model Parameters

The motion of the cervical spine comprises flexion and extension, lateral bending and axial rotation. Hence, in order to obtain full spine mobility, the model for the vertebrae pair must allow for relative six-degree-of-freedom motion, even in the presence of kinematical constraints, as specified below. As only relative motion interests in this setting, the lower vertebra C6 is fixed to the inertia system, to which the upper vertebra C5 is connected via a six-degree-of-freedom joint with three translations along the coordinate axes and three (consecutive) rotations about the same axes. In addition to the six-degree-of-freedom joint, motion constraints are introduced by (unilateral) contact elements reproducing the surfaces of the facet joints. Moreover, the junction between the vertebrae is enforced by force-displacement elements comprising the intervertebral disc and the ligaments, as explained below.

Structure and Inertia Properties

The definition of the reference coordinate systems is depicted in Figure 1. The x-axis points to the front and the z-axis upwards. Table 1 summarizes the initial translations, s_x, s_z, of the origin of the upper body in x- and z-direction, respectively, and the relative rotation φ_y about the y-axis with respect to the lower body. The table also displays the inertia properties of the vertebrae.

body	mass	tensor of inertia			origin		COG	orient.
	m	I_{xx}	I_{yy}	I_{zz}	s_x	s_z	g_x	φ_y
	kg	kg · cm^2			mm		mm	deg
C5	0.23	2.3	2.3	4.5	-2.8	17.4	-8.1	-5.2
C6	0.24	2.4	2.4	4.7	-2.0	18.4	-8.3	-5.6

Table 1. Inertia properties (de Jager).

Intervertebral Disc

The intervertebral disc can be modeled by an anisotropic set of parallelly connected linear spring-damper elements. These elements incorporate also the effects of the uncovertebral joints. The force-displacement properties of the intervertebral disc are computed as follows:

$$
\begin{aligned}
F_x &= \begin{cases} k_{x+}\, t_x + b_t\, v_x & : \quad t_x \geq 0 \\ k_{x-}\, t_x + b_t\, v_x & : \quad t_x < 0 \end{cases} \\
F_z &= k_y\, t_y + b_t\, v_y \\
F_z &= \begin{cases} k_{z+}\, t_z + b_t\, v_z & : \quad t_z \geq 0 \\ k_{z-}\, t_z + b_t\, v_z & : \quad t_z < 0 \end{cases} \\
M_x &= k_{\varphi_x}\, \varphi_x + b_\varphi\, \omega_x \\
M_y &= \begin{cases} k_{\varphi_{y+}}\, \varphi_y + b_\varphi\, \omega_y & : \quad \varphi_y \geq 0 \\ k_{\varphi_{y-}}\, \varphi_y + b_\varphi\, \omega_y & : \quad \varphi_y < 0 \end{cases} \\
M_z &= k_{\varphi_z}\, \varphi_z + b_\varphi\, \omega_z
\end{aligned}
\tag{1}
$$

with $\mathbf{F} = \left[F_x\ F_y\ F_z \right]^T$ denoting the resulting force at the disc midpoint, t_x, t_y, t_z denoting the deflections along the coordinate axes, v_x, v_y, v_z denoting their respective time derivative, $\mathbf{M} = \left[M_x\ M_y\ M_z \right]^T$ denoting the resulting torque vector, $\varphi_x, \varphi_y, \varphi_z$ denoting the small angular rotations about the coordinate axes, and $\omega_x, \omega_y, \omega_z$ denoting their respective time derivative. The numerical values for the stiffness coefficients are taken from Moroney et al. (1988) and are summarized in Table 2. The load directions correspond to the six degrees of freedom of the relative motion of the vertebrae pair, namely anterior shear (AS) and posterior shear (PS) for x translation, lateral shear (LS) for y translation, tension (TNS) and compression (CMP) for z translation, lateral bending (LB) for x rotation, flexion (FLX) and extension (EXT) for y rotation, and axial rotation (AR) for z rotation. The damping coefficients for translation and rotation were taken as $b_t = 1000$ Ns/m and $b_\varphi = 1.5$ Nms/rad according to de Jager (1996).

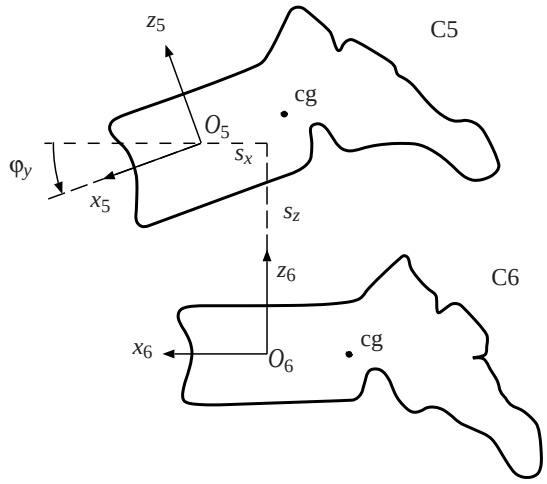

Figure 1. Definition of the reference systems.

Facet Joints

In addition to the intervertebral disc, the vertebrae pair is partially guided by the facet joints. These joints support only pressure contact forces and hence act as unilateral constraints comprising contact and free-flight phases. During contact, the roughly planar surfaces of the contact pair glide on each other with almost no friction. When the contact force vanishes, the surfaces detach from each other, eliminating the geometric constraints induced by the facet joint temporarily. During this motion, the facet joints are pulled together by the surrounding ligaments, which act as force elements.

coefficient	k_{x+}	k_{x-}	k_y	k_{z+}	k_{z-}	k_{φ_x}	$k_{\varphi_{y+}}$	$k_{\varphi_{y-}}$	k_{φ_z}
direction	AS	PS	LS	TNS	CMP	LB	FLX	EXT	AR
of load	N/mm					Nm/deg			
stiffness	62	50	73	68	492	0.33	0.21	0.32	0.42

Table 2. Stiffness properties of intervertebral disc (Moroney et al. 1988).

In order to be able to reproduce the synovial behavior of the facet joints, the latter were modeled as frictionless compliant contact elements allowing for normal compression and producing contact forces depending linearly on normal penetration and its time derivative.

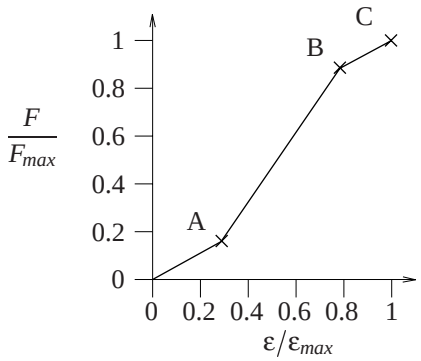

Figure 2. Force-strain curve.

The normal contact force F_c hence is determined by

$$F_c = b_f \cdot \dot{u} + \\ + \begin{cases} 2 \cdot 10^9 \mathrm{N/m^2} \cdot u^2 & : \ 0 \le u \le 3 \cdot 10^{-4}\mathrm{m} \\ 180\,\mathrm{N} + 1.2 \cdot 10^6 \mathrm{N/m} \cdot (u - 3 \cdot 10^{-4}\mathrm{m}) & : \ u > 3 \cdot 10^{-4}\mathrm{m} \end{cases},$$

where u represents the penetration, in meters, and $\dot{u}$ is the penetration rate, as measured in m/s. The damping coefficient b_f is set to $b_f = 300$ Ns/m according to de Jager (1996).

Nonlinear Viscoelastic Ligaments

Six ligaments of the lower cervical spine are incorporated in the model, namely, the anterior longitudinal ligament (ALL), the posterior longitudinal ligament (PLL), the flaval ligament (FL), the interspinous ligament (ISL) and the left and right capsular ligament (CL).

The ligaments are modeled as *robes* transmitting only tension forces. These tension forces are functions of ligament elongation ε and its time derivative, namely

$$F_l = \begin{cases} F_{el}(\varepsilon) + b_l \cdot \mathrm{d}\varepsilon/\mathrm{d}t & : \ \varepsilon \ge 0 \\ 0 & : \ \varepsilon < 0 \end{cases},$$

where the load-displacement curves $F_{el}(\varepsilon)$ are taken as piecewise linear functions comprising three segments, as shown in Figure 2. The corresponding numerical values of the support points A, B, C taken in this report are reproduced in Table 3, while the damping coefficient b_l was set to 300 Ns/m, corresponding to given patterns in the literature. The lengths of the ligaments in the undeflected case, l_0, can be found in Table 4 together with the corresponding assumed insertion points of the ligaments in body-fixed coordinates of the coordinate frame of the corresponding vertebra body.

	A		B		C	
	$\frac{\varepsilon}{\varepsilon_{max}}$	$\frac{F}{F_{max}}$	$\frac{\varepsilon}{\varepsilon_{max}}$	$\frac{F}{F_{max}}$	ε_{max}	$\frac{F_{max}}{\mathrm{N}}$
ALL	0.24	0.11	0.80	0.88	0.58	111
PLL	0.22	0.12	0.78	0.90	0.45	83
FL	0.33	0.21	0.77	0.89	0.21	115
ISL	0.33	0.19	0.78	0.87	0.40	34
CL	0.28	0.16	0.78	0.88	0.42	108

Table 3. Ligament parameters for spinal level C5–C6 (de Jager 1996); see also Figure 2.

	origin C5			origin C6			
	x	y	z	x	y	z	l_0
ALL	7.7	0.0	0.0	8.0	0.0	0.0	18
PLL	-8.1	0.0	0.0	-8.3	0.0	0.0	17
FL	-25.4	0.0	-1.7	-26.3	0.0	-1.9	15
ISL	-39.9	0.0	-3.2	-47.3	0.0	-4.1	16
CL	-15.1	±20.3	-5.1	-12.9	±20.0	7.2	6

Table 4. Ligament insertion points for spinal level C5–C6 (x, y, z, l_0 in mm) (de Jager 1996).

Madymo Model

In order to obtain a reference computer model for the kinematic, static and dynamic behaviour of the vertebrae pair, the world-wide standard package MADYMO for occupant safety analysis was employed, using the data set given in the previous section. The facet joints were implemented as `Ellipsoid-Ellipsoid Contact Interactions`. For visualization purposes, vertebrae bodies were modeled also as hyper-ellipsoids, but with no contact interactions. Similarly, the vertebra arches are visualized as elongated hyper-ellipsoids. Moreover, in order to reduce computational overhead, only the hyper-ellipsoids embodying the facet joints are graphically rendered, without reproduction of the interconnection to the vertebra bodies. This crude graphical model suffices to verify motion results, while at the same time yielding acceptable simulation times for the computer runs (approx. 5.7 seconds per run on an SGI workstation; CPU: MIPS R10000, 175 MHz). The visco-elastic behavior of the intervertebral disc was realized by restraining the origins of the vertebra body reference systems by `Point-Restraints` for the translational part and by `Cardan Restraints` for the rotational part. Six ligaments

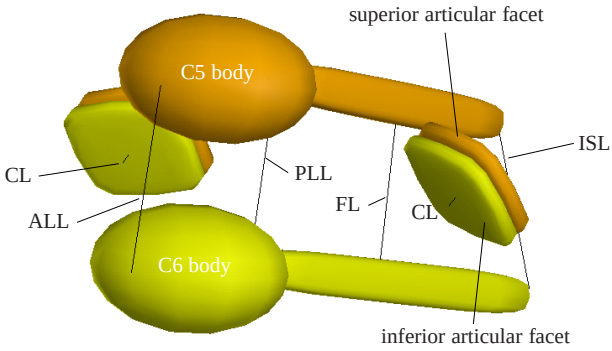

Figure 3. C5–C6 MADYMO ellipsoid model

modeled as `Kelvin Elements` were additionally regarded.

MBILE Model

Although the MADYMO-model was valuable in producing accurate simulation results for the regarded vertebrae-pair motion, excessive simulation time turned out to be a mayor drawback in analyzing different parameter sets quickly, or even an online simulation. Hence, an alternative model of the vertebrae pair interactions was developed using the object-oriented multibody package MBILE (Kecskeméthy 1999) and extensions hereof, as described below.

Serial Model

For the relative kinematics between the two vertebrae bodies without regard of the facet joints, a six-degree-of-freedom joint comprising the concatenation of three translational joints and three rotational joints was employed. The particular modeling of the facet joints is explained in the following sections.

For visualization purposes, two graphic rendering models were regarded. One simplified model comprises only cones, cylinders and spheres, giving a rough idea of the vertebrae locations (Figure 4). The other graphic rendering model employs original 3D vertebra visual geometry from Viewpoint® Digital™ and hence renders a more realistic view of vertebrae motion, which can be used for example for understanding the effects of implants or for training purposes (Figure 6). Both models build upon the *OpenInventor* features of an SGI workstation and are completely independent of the contact iterations. Hence, the user can switch easily between them by making an appropriate selection in the operation interface. In contrast to the MADYMO model, the MBILE software package allows online user interactions during the animation. This is achieved through software slider controls, by which system parameters can be changed interactively (Figure 5). For example,

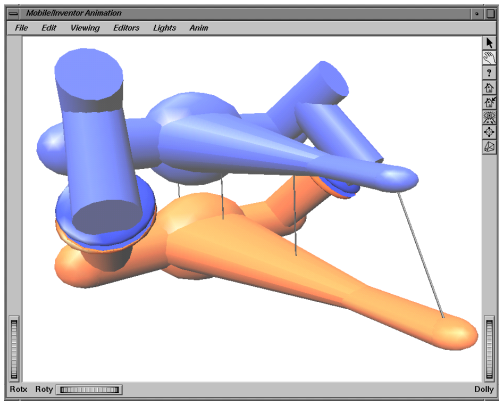

Figure 4. MOBILE model with simplified graphics.

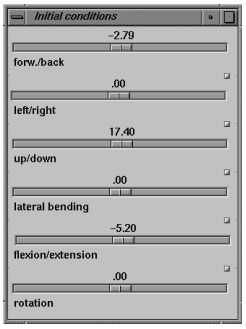

Figure 5. MOBILE Slider.

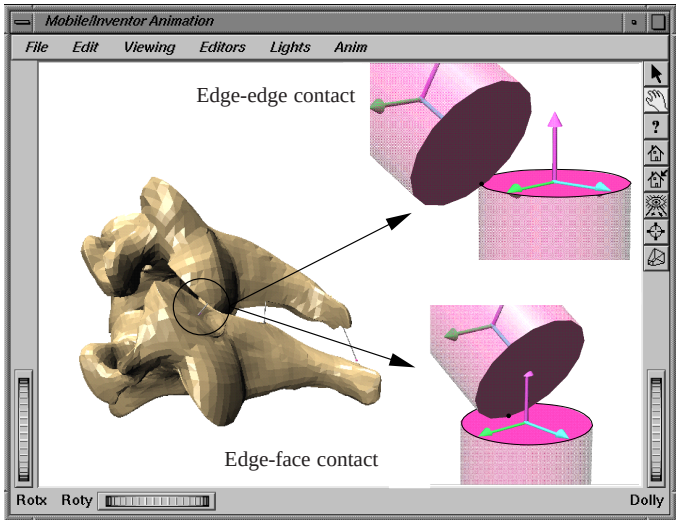

Figure 6. MOBILE model.

the mechanism response can be controlled visually while stiffness properties of the intervertebral disc are changed.

Impact Analysis

In order to obtain efficient and accurate computer models, a set of impact geometry situations was investigated by regarding the facet joints as the end faces of two cylinders in contact with each other. This assumption seems justified due to the almost flat shape of the articulated surfaces, and proved to be sufficiently accurate in the ensuing simulations. In this setting, four possible contact situations may occur: (1) the edge of the upper cylinder touches the flat end of the lower cylinder (Figure 6, right bottom); (2) the edge of the upper cylinder touches the egde of the lower cylinder (Figure 6, right top); (3) the edge of the lower cylinder touches the flat end of the upper cylinder; and (4) both flat ends of the cylinders rest flatly upon each other.

For edge-edge contact, referring to Figure 7, the following relationships hold:

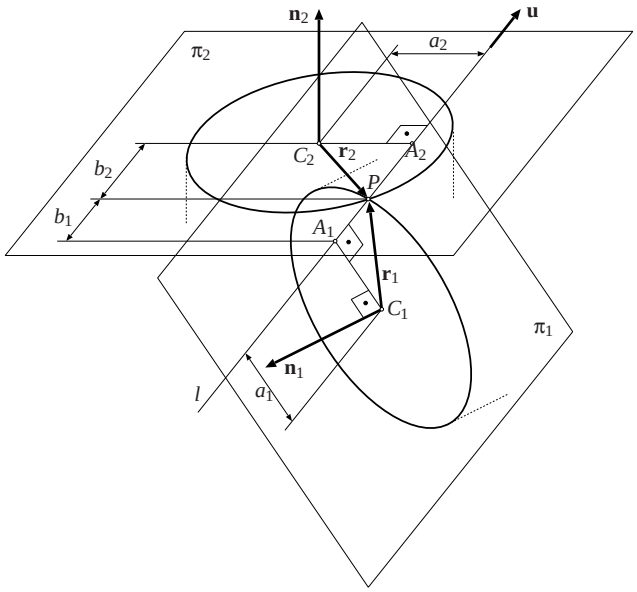

Figure 7. Frictionless circle-circle contact.

Let r_1 and r_2 be the radii of the circles. Moreover, let a_1 and a_2 be the distances from the center points of the two circles to the common line of intersection of the disc planes π_1 and π_2. One obtains

$$a_1 = \frac{(\mathbf{c}_2 - \mathbf{c}_1)\cdot\mathbf{n}_2}{\mathbf{u}_{a1}\cdot\mathbf{n}_2} = \frac{\mathbf{c}\cdot\mathbf{n}_2}{\mathbf{u}_{a1}\cdot\mathbf{n}_2}\,,\quad a_2 = \frac{(\mathbf{c}_1 - \mathbf{c}_2)\cdot\mathbf{n}_1}{\mathbf{u}_{a2}\cdot\mathbf{n}_1} = -\frac{\mathbf{c}\cdot\mathbf{n}_1}{\mathbf{u}_{a2}\cdot\mathbf{n}_1}\,,$$

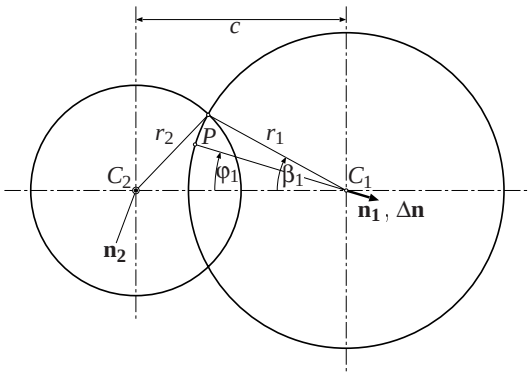

Figure 8. Projection onto contact plane for flat contact.

where $\mathbf{c} = \mathbf{c}_2 - \mathbf{c}_1$ is the vector from C_1 to C_2, $\mathbf{n}_1$ and $\mathbf{n}_2$ are the plane normals of circle 1 and 2, respectively, and $\mathbf{u}_{a1}$ and $\mathbf{u}_{a2}$ are unit vectors in direction of the perpendicular distance from the circle midpoints C_1 and C_2 to the common line of intersection of the disc planes, respectively.

Using the quantities described above, the distances b_1 and b_2 from the feet of the circle midpoints at the common line of intersection of the disc planes to the contact point P can be readily computed as

$$b_{1,2} = \sqrt{{r_{1,2}}^2 - {a_{1,2}}^2} \ .$$

Note that b_1 and b_2 are real whenever the common line of intersection of the disc planes intersects both circles. The distance d between the circles along the common line of intersection of the disc planes can be computed as

$$d = |\mathbf{c}\cdot\mathbf{u}| - (b_1 + b_2); \ \ d < 0 : \text{penetration}$$

where $\mathbf{u}$ is the unit vector in direction of the common line of intersection of the disc planes. At contact, $d = 0$, the contact condition becomes

$$b_1 + b_2 = |\mathbf{c}\cdot\mathbf{u}| \ .$$

In the case of an almost flat contact between the cylinder surfaces, the formulas derived above become singular. In this case, one can establish the contact geometry by projecting the circles on the plane normal to the (almost parallel) cylinder axes.

In the following, first the case of contact between the edge of circle 1 and the flat end surface of cylinder 2 is regarded (Figure 8). The case of contact between circle 2 and the end surface of cylinder 1 is treated analogously. Let P be the contact point and assume that the projection plane is taken as π_2. The inclination of cylinder 1 with respect to cylinder 2 is assumed to be so small that the distortion of circle 1 to an ellipse is negligible. Contact is maintained whenever the angle φ_1 subtended between the interconnection line of the two circle centers and the ray passing through C_1 and the contact point is less than or equal the angle β_1 subtended between the circle interconnection line and the ray passing through C_1 and the intersection point of both circles.

For the angle β_1, one readily obtains

$$r_2^2 = r_1^2 + c^2 - 2\,r_1\,c\cos\beta_1 \ \Rightarrow \ \cos\beta_1 = \frac{1}{2\,r_1\,c}\left(r_1^2 - r_2^2 + c^2\right) \ ,$$

where $c = \overline{C_1 C_2}$. The angle φ_1 can be calculated as

$$\cos\varphi_1 = \frac{-\mathbf{c}\cdot\Delta\mathbf{n}}{|\mathbf{c}|\,|\Delta\mathbf{n}|} ,$$

with $\Delta\mathbf{n} = \mathbf{n}_1 + \mathbf{n}_2$, a quantity that would correspond to the "difference" of the circle normals when both were oriented towards the same half-space. However, by taking into account that at contact the surface normals of the two touching cylinders are faced opposite to each other, the above mentioned difference actually becomes the sum of the cylinder normals.

By inserting the above expressions in the contact condition $\cos\varphi_1 \geq \cos\beta_1$, one obtains as condition for a contact of the edge of circle 1 on the end surface of cylinder 2, or similarly for a contact of the edge of circle 2 on the end surface of cylinder 1, respectively

$$-\mathbf{c}\cdot\Delta\mathbf{n} \geq \frac{1}{2}\frac{|\Delta\mathbf{n}|}{r_1}\left(r_1^2 - r_2^2 + c^2\right) \quad \text{or,}$$
$$\mathbf{c}\cdot\Delta\mathbf{n} \geq \frac{1}{2}\frac{|\Delta\mathbf{n}|}{r_2}\left(r_2^2 - r_1^2 + c^2\right) \ .$$

By regarding the expression for $\cos\beta_1$ above, the following case distinctions can be made:

$$\frac{(r_1^2 - r_2^2 + c^2)}{2\,r_1\,c} \ \begin{cases} > 1 : \text{(virtual) contact outside of disc 2} \\ < -1 : \text{disc 1 fully contained in disc 2} \\ \text{else} : \text{partial overlapping of discs 1 and 2} \end{cases} ,$$

By the same token, after establishing a similar expression for

$\cos\beta_2$, one obtains the case distinctions

$$\frac{(r_2^2 - r_1^2 + c^2)}{2\,r_2\,c} \quad \begin{cases} > 1 : \text{(virtual) contact outside of circle 1} \\ < -1 : \text{disc 2 fully contained in disc 1} \\ \text{else} : \text{partial overlapping of discs 2 and 1} \end{cases} .$$

The above derived formulas fail to be applicable when the circles are fully parallel because in this case the vector $\Delta\mathbf{n}$ vanishes. For this case, one can assume the contact to take place at the center point M of the segment of the center interconnection line contained in the common contact patch (for partially overlapping discs). The distance between C_1 and M is given by

$$L = c - r_2 + \frac{r_1 + r_2 - c}{2} = \frac{c + r_1 - r_2}{2} .$$

If disc 1 lies completely within disc 2, one can assume that the contact point M coincides with C_1. Correspondingly, one can define the contact point M as incident with C_2 when disc 2 lies completely within disc 1.

For smooth transition between the fully parallel case and the almost parallel case, a novel procedure is proposed, where a virtual contact point is obtained by interconnecting M and P and employing a blending function to position the virtual contact point between these two extremes as a function of the angle between the circle normals. The blending function chosen in the present context is

$$r = r_0\,(1 - e^{-C\sin\alpha}) \quad ,$$

with r_0 being the distance between M and P, C a constant and α the subtended angle between the circle normals. The basic idea

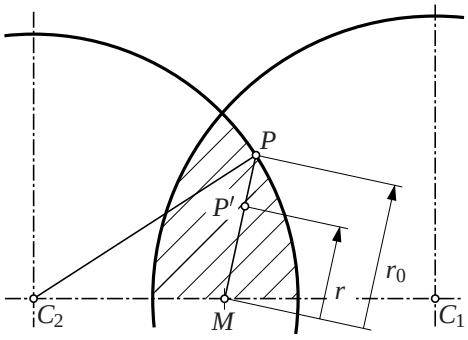

Figure 9. Blending ray within contact patch for flat cylinder-cylinder contact.

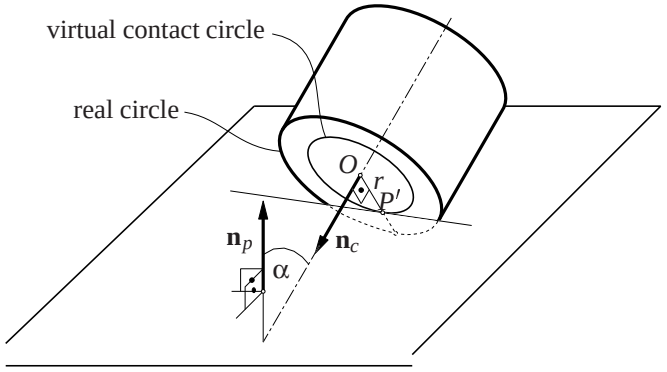

Figure 10. Disc-plane contact.

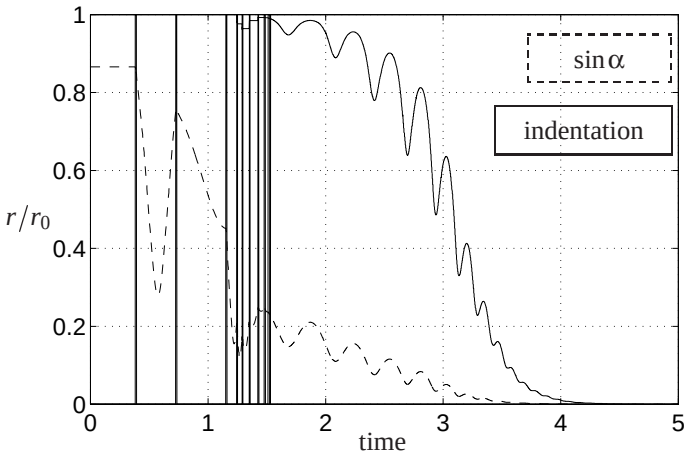

Figure 11. Smooth steep-to-flat transition.

of the blending function is illustrated in Figure 10 for the case of a contact of a cylinder with a plane. The virtual contact point P' lies between the center of the cylinder and its circumference along the line of intersection of the common plane of the surface normals $\mathbf{n}_p$ and $\mathbf{n}_c$ and the cylinder end surface through the center of the circle. A particular property of the blending function used is that it renders a stabilizing moment in direction perpendicular to both surface normals that makes fully stable flat contact possible. Hence, no further computations and state transition tracking procedures are necessary for transition from steep to flat contact as well as for transition from one edge to the other. A result of a simulation of the contact between a disc and a plane is displayed in Figure 11, where the relative indentation r/r_0 (with r_0 being the original disc radius and r the actual distance to the circle center) and the sine of the inclination angle α are plotted over time. Clearly, the motion asymptotically approaches fully flat contact with the virtual contact point at the circle center.

Forces As frictionless contact is assumed, the contact force must be aligned with the common line of intersection of the disc planes. In order to take account also of penetration situations, a positive penetration distance d is assumed. The vector $\mathbf{r}_1$ from C_1 to the contact point P is then assumed as

$$\mathbf{r}_1 = a_1 \cdot \mathbf{u}_{a1} + (b_1 + \frac{d}{2}) \cdot \mathbf{u},$$

where the term $d/2$ makes P lie in the middle between the two intersection points of the circles with the corresponding end face planes. Note that for this to hold true the vector $\mathbf{u}$ must be chosen such that $\mathbf{c} \cdot \mathbf{u} > 0$. This can always be assured by choosing an appropriate sign in the formula for calculation of $\mathbf{u}$, i.e., in

$$\mathbf{u} = \pm \frac{\mathbf{n}_1 \times \mathbf{n}_2}{\| \mathbf{n}_1 \times \mathbf{n}_2 \|} \quad .$$

The position of P with respect to C_2 is obtained accordingly by the vector $\mathbf{r}_2 = \mathbf{r}_1 - \mathbf{c}$.

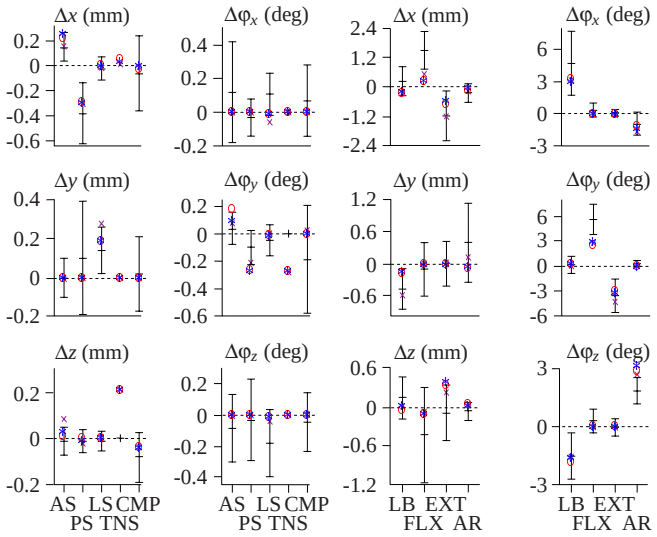

Figure 12. Model comparison of main and coupled displacements: MBILE: ○, MADYMO: ∗, de Jager (1996): × with experimental results of Moroney et al. (1988): + (average± SD).

Model Validation

Both vertebrae pair models developed with the MADYMO package and the MBILE library were compared and validated with the experimental results reported by Moroney (Moroney et al. 1988) and the computer simulation performed by de Jager (de Jager 1996). The simulations compute the translational and rotational deflections from the reference position of vertebra C5 to the new state of equilibrium for nine loading conditions corresponding to the application of a single force (20 N) or moment (1.8 Nm) in direction of each elementary motion of C5. In this setting, the numerical values shown in Figure were obtained. As it can be seen, a good agreement between the experimental data and the computer models could be achieved. In particular, the simplified MBILE model renders results that are not more inaccurate than the complex MADYMO model. At the same time the MBILE model turns out to be faster then the MADYMO model by a factor of 350 (SGI workstation MIPS R10000).

The reason for this performance enhancement is that, besides using simpler and more efficient mathematical models of the contact mechanics, the calculation of the static equilibrium could be achieved in MBILE in a few iterations using the built-in object `MoStaticEquilibriumFinder`, which works with a Newton-Raphson algorithm. In contrast to this, the MADYMO model required the computation of dynamics for the movable vertebra C5 to approach equilibrium.

Conclusions and Outlook

With the simplified contact model of facet joints using cylinder-cylinder pairs, a highly efficient and sufficiently accurate model for intervertebral motion could be achieved. This high performance model may be useful in applications were several traversals of the kinematics, statics and/or dynamics are required, as e.g. for parameter estimation purposes, or in a controller for a physical model of a vertebrae pair, employing, for example, miniaturized parallel platform of Gough-Steward type. The latter application is planned for future work.

ACKNOWLEDGMENT

The support of the present work by the European Community as a Marie Curie Research Training Grant ERBFMBICT983385 is gratefully acknowledged.

REFERENCES

Bedewi, P. G. and Bedewi, N. E., 1996, "Modeling of occupant biomechanics with emphasis on the analysis of lower extremity injuries, " *International Journal of Crashworthiness*, Vol. 1, No. 1.

Bilston, L. E. and Thibault, L. E., 1996, "The mechanical properties of the human cervical spinal cord in vitro, " *Annals of Biomedical Engineering*, Vol. 24, pp. 67–74.

Bothema, R. and Roth, B., 1990, *Theoretical Kinematics*, Dover.

de Jager, M., 1996, "Mathematical head-neck models for acceleration impacts, " PhD thesis, Technische Universiteit Eindhoven.

DiAngelo, D., Jansen, T., Eckstein, E., Dull, S. and Foley, K., 1996, "Biomechanical analysis of the C1-C2 transarticular

screw fixation technique., " *Advances in Bioengineering*, Vol. BED-Vol. 33.

Geigl, B. C., Steffan, H., Dippel, C., Muser, M. H., Walz, F. and Svensson, M. Y., 1995, "Comparison of head-neck kinematics during rear end impact between Standard Hybrid III, RID Neck, volunteers and PMTOs, " *Proceedings of the 1995 International IRCOBI Conference on the Biomechanics of Impacts*, Brunnen, Switzerland, pp. 261–270.

Jansen, T. H. and DiAngelo, D., 1997, "Influences of the location of vertebral IAR on cervical spine kinematics, " *Proceedings of 16th Southern Biomedical Engineering Conference, Biloxi, MS*, Dept. of Biomedical Engineering, University of Tennessee.

Kecskeméthy, A., 1999, MOBILE 1.3 user's guide, Institut für Mechanik und Getriebelehre, Technische Universität Graz.

Lupker, H. A., de Coo, P. J. A., Nieboer, J. J. and Wismans, J., 1991, "Advances in MADYMO crash simulations, " Technical Report No. 910879, SAE.

Margulies, S. S., Meaney, D. F., Bilston, L. B., Riederer, S. R. and Campeau, N. C., 1992, "In vivo motion of the human cervical spine cord in extension and flexion, " *Proceedings of the 1992 IRCOBI Conference*, Verona, Italy, pp. 213–224.

Moroney, S. P., Schultz, A. B., Miller, J. A. A. and Anderson, G. B. J., 1988, "Load-displacement properties of lower cervical spine motion segments, " *Journal of Biomechanics*, Vol. 21, pp. 769–779.

Obergefell, L. A., Gardner, T. R., Kaleps, I. and Fleck, J. T., 1988, Articulated total body model enhancements: User's guide, Armstrong Aerospace Medical Research Laboratory. Report No. AAMRL-TR-88-043.

White, A. and Panjabi, M. M., 1990, *Clinical Biomechanics of the Spine*, second edn, J. B. Lippincott.

Wismans, J., van Oorschot, H. and Wotering, H. J., 1986, "Omni-directional human head-neck response, " SAE Paper No. 861893, Society of Automotive Engineers.